Dynamic pneumococcal genetic adaptations support bacterial growth and inflammation during coinfection with influenza

Amanda P. Smith[1], Lindey C. Lane[1], Tim van Opijnen[2], Stacie Woolard[3], Robert Carter[4], Amy Iverson[5], Corinna Burnham[5], Peter Vogel[6], Dana Roeber[7], Gabrielle Hochu[1], Michael D.L. Johnson[8], Jonathan A. McCullers[1], Jason Rosch[5*], Amber M. Smith[1*]

[1]Department of Pediatrics, University of Tennessee Health Science Center, Memphis, TN 38163 USA
[2]Department of Biology, Boston College, Chestnut Hill, MA 02467 USA
Departments of [3]Flow Cytometry, [4]Oncology, [5]Infectious Diseases, [6]Pathology, [7]Hartwell Center, St. Jude Children's Research Hospital, Memphis, TN 38105 USA
[8]Department of Immunobiology, University of Arizona, Tucson, AZ 85724 USA

* amber.smith@uthsc.edu , jason.rosch@stjude.org

Abstract

Streptococcus pneumoniae (pneumococcus) is one of the primary bacterial pathogens that complicates influenza virus infections. These secondary infections increase influenza-associated morbidity and mortality through a number of immunological and viral-mediated mechanisms. However, little is known about how specific bacterial genes contribute to post-influenza pathogenicity. Thus, we used genome-wide transposon mutagenesis (Tn-Seq) to reveal bacterial genes conferring improved fitness in influenza infected hosts. The majority of the 32 identified genes are involved in bacterial metabolism, including nucleotide biosynthesis, amino acid biosynthesis, protein translation, and membrane transport. We investigated five of the genes in detail: SPD1414, SPD2047 (*cbiO1),* SPD0058 (*purD*), SPD1098, and SPD0822 (*proB*). Single-gene deletion mutants showed slight growth attenuations *in vitro* and *in vivo*, but still grew to high titers in both naïve and influenza-infected murine hosts. Despite high bacterial loads in the lung and sustained bacteremia, mortality was significantly reduced or delayed with each of the knockouts. Reductions in pulmonary neutrophils, inflammatory macrophages, and select proinflammatory cytokines and chemokines were observed at discrete times after coinfection with

these bacterial mutants. Immunohistochemical staining also revealed altered neutrophil phenotype and distribution in the lungs of animals coinfected with knockouts. These studies demonstrate a critical role for specific bacterial genes in driving virulence and immune function during influenza-associated bacterial pneumonia.

Author Summary

Streptococcus pneumoniae (pneumococcus) is a common coinfecting pathogen that increases morbidity and mortality during influenza epidemics and pandemics. It is known that the strain, dose, and timing of bacterial coinfection influence the likelihood of severe pneumonia, but the specific bacterial genes that contribute to bacterial pathogenicity during influenza coinfection remain unknown. Using a genome-wide analysis, we identified the pneumococcal genes that exacerbate disease during influenza-bacterial coinfection. Most of these have a role in metabolism. To better understand their contribution to this lethal disease, we generated 5 mutants that lacked a single gene. The strains grew to high titers in the lungs and blood of both healthy and influenza-infected animals yet mortality was significantly reduced. In influenza-infected animals, there was also significantly lower inflammatory immune responses, and lung pathology. These important pneumococcal adaptations largely facilitate lethality during influenza-pneumococcal coinfection. Investigating whether similar metabolic adaptations are conserved among bacterial species that complicate influenza could yield broadly effective therapies that abrogate lethal post-influenza bacterial infections.

Introduction

Bacterial pathogens often complicate influenza virus infections, causing increased morbidity and mortality. *Streptococcus pneumoniae* (pneumococcus) is one of the leading pathogens causing death in influenza-infected hosts (1-3). During past pandemics, pneumococcal infection has presented as a risk factor for hospitalization and severe disease and has accounted for a significant proportion of influenza-related deaths (4-7). There is considerable genetic diversity within and between pneumococcal serotypes, and laboratory and clinical studies suggest that specific strains are preferentially promoted in influenza-infected hosts (8-10). Despite the clinical importance of this synergy, the bacterial factors that contribute to coinfection disease severity have yet to be determined in a systematic way.

During influenza A virus (IAV) coinfection with pneumococcus, bacteria are able to grow rapidly, viral burden increases, and significant inflammation amasses (Reviewed in references 11-16). The host-pathogen interplay is complex with numerous factors contributing to pathogen growth and host disease. Several studies have investigated the impact of viral virulence factors (17-25), bacterial virulence factors (23, 26), and host immune responses (Reviewed in references 11-15, 21, 27) to the pathogenicity of bacterial coinfections during influenza infection. Incidence of coinfection is, in part, a function of the detrimental effects that influenza virus infection has on key immune responses. Initial pneumococcal invasion and growth kinetics are regulated by virus induced depletion (28-31) or dysfunction (31-33) of alveolar macrophages (AMΦ), depending on the animal model (31). That is, the ratio of functional AMΦ and bacteria determines the initial bacterial growth phenotype and bacterial concentration increases when AMΦ become sufficiently limited in their capacity to phagocytose bacteria and, thus, provide sustained protection (30). Additional functional defects in AMΦ, neutrophils, and inflammatory macrophages are also present and likely contribute to sustained bacterial burden (31, 34-42). Several studies indicate

that influenza-bacterial coinfection disease severity results from an immune 'storm', characterized by abundant immune cell infiltration and hyper-production of damaging pro-inflammatory cytokines (Reviewed in references 12-16, 21, 43). However, it remains unclear how specific bacterial species and/or strains influence these immune responses and coinfection pathogenicity.

Direct investigation into known pneumococcal virulence factors in influenza-infected hosts has provided some support that the bacteria need to adapt to a changing environment (22, 25). In the nasopharynx, bacterial sialic acid catabolism genes are important for enhanced bacterial growth during influenza virus infection (25). This may be a consequence of increased sialic acid availability mediated by viral and/or bacterial neuraminidases (NA)(25). Although viral NA can increase bacterial attachment to infected cells (18, 44), this does not seem to contribute significantly to bacterial growth (29). However, bacterial interactions with virus-infected cells do have a role in other aspects of the infection, including the viral rebound often observed post-bacterial coinfection (18, 29).

During primary pneumococcal infection, several genes have been identified as important regulators of disease severity (Reviewed in references 45-47). Systematic genomic screens have not yet been employed to assess pneumococcal adaptations during influenza coinfection. However, they were used to investigate which genes were necessary for growth of *Haemophilus influenzae* in the presence of influenza virus (48). Several influenza-induced metabolic adaptations of *H. influenzae* were identified, including changes in purine biosynthesis, amino acid metabolism, iron homeostasis, and cell wall synthesis (48). Genomic screens assessing pneumococcal adaptations in the context of other comorbidities have suggested similar alterations. For example, in hosts with sickle cell anemia, pneumococcal alterations in the TIGR4 strain included genes involved in complement function, iron acquisition, and purine biosynthesis (49). Given these important findings and the similar adaptations in bacterial metabolism under

various host pressures, understanding how bacterial genes influence influenza-pneumococcal coinfection is critical and could identify mechanisms conserved across bacterial species amenable to targeting with therapeutics.

Here, we sought to identify specific pneumococcal genes that affect pathogenicity in influenza-infected hosts. To investigate this question, we used the genome-wide tool transposon insertion sequencing (Tn-Seq)(50) to reveal genotypes that confer bacterial fitness during viral coinfection compared to primary bacterial infection. This analysis identified 32 genes, most with metabolic functions, that contribute to pneumococcal fitness during influenza coinfection and do so in a time-dependent manner. To determine how select genes affect pathogenicity and host immune functions, we generated 5 single-gene deletion mutants (D39Δ*cbiO1*, D39Δ*purD*, D39Δ*1414*, D39Δ*1098*, and D39Δ*proB*). The lethality of these knockout strains was significantly reduced in influenza-coinfected animals and significantly reduced or eliminated in naïve animals. This improvement in survival occurred despite high bacterial loads in the lungs and blood. However, select host immune responses were significantly suppressed, pulmonary consolidation was reduced, and pulmonary neutrophils had a more intact, functional morphology when pneumococci lacked these genes during influenza-coinfection. Taken together, these data indicate a critical role for pneumococcal metabolism in shaping host responses and disease severity during post-influenza bacterial pneumonia.

Results

Bacterial Adaptations During Pneumococcal Coinfection With Influenza

To identify which pneumococcal factors are required for growth during IAV infection, we employed a high-throughput, transposon sequencing (Tn-Seq) approach (50). We generated a pool of ~50,000 mutants in the type 2 pneumococcal strain D39, then infected groups of mice with 75

$TCID_{50}$ influenza A/Puerto Rico/34/8 (PR8) or mock control (PBS) followed 7 d post infection (pi) with 1e6 CFU of the mutant library. Lungs were harvested at 12 h or 24 h post-bacterial infection (pbi) and the bacteria were collected, genomic DNA was isolated and sequenced, and the relative abundance and fitness of mutants was calculated (details in Supplementary Information). In comparing the results from pre- and post-infection and from IAV- and PBS-infected animals, 17 genes conferred differential fitness at 12 h, and 23 genes had differential fitness at 24 h pbi. Of these, 8 genes were detected at both time points (Table 1, Fig 1).

The core set of genes identified at both 12 h and 24 h pbi are responsible for amino acid biosynthesis, nucleotide biosynthesis, protein translation, and membrane transport (Fig 1). Genes in the purine biosynthesis pathway comprised the largest number of genes (8 total; SPD0002 (*dnaN*), SPD0052, SPD0053 (*purF*), SPD0054 (*purM*), SPD0055 (*purN*), SPD0057 (*purH*), SPD0058 (*purD*), and SPD0059 (*purE*)) followed by ATP-binding cassette (ABC) transporters (5 total; SPD1098, SPD1099, SPD2047 (*cbiO1)*, SPD2048 (*cbiO2*), and SPD1354 (putative)), protein translation (6 total; SPD0395 (*efp*), SPD1782 (*ksgA*), SPD0907 (hemK), SPD1130 (licD2), SPD1293, SPD1923), and proline biosynthesis (3 total; SPD0822 (*proB*), SPD0823 (*proA*), SPD0824 (*proC*)). Other genes included a putative membrane protein (SPD1090), carbon metabolism (SPD0723 (*ripA*), SPD1087, SPD1333 (putative), and SPD1468), and riboflavin metabolism (SPD0994).

Table 1: Pneumococcal Genes with Significant Differential Fitness During Coinfection with Influenza A Virus. Pneumococcal genes identified at 12 h and 24 h pbi by Tn-Seq (see Materials and Methods) as important for pneumococcal growth during IAV infection compared to a naïve infection. Highlighted in bold are the genes chosen for additional characterization.

Locus	Gene	Description	12 h	24
SPD_0002	dnaN	DNA polymerase III subunit beta	√	
SPD_0052		phosphoribosylformylglycinamidine synthase, putative		√
SPD_0053	purF	amidophosphoribosyltransferase		√
SPD_0054	purM	phosphoribosylformylglycinamidine cyclo-ligase		√
SPD_0055	purN	phosphoribosylglycinamide formyltransferase	√	√
SPD_0057	purH	bifunctional purine biosynthesis protein PurH	√	√
SPD_0058	**purD**	**phosphoribosylamine--glycine ligase**	**√**	**√**
SPD_0059	purE	phosphoribosylaminoimidazole carboxylase, catalytic subunit	√	√
SPD_0182		conserved hypothetical protein	√	
SPD_0372		sodium:alanine symporter	√	√
SPD_0395	efp	translation elongation factor P		√
SPD_0723	rpiA	ribose 5-phosphate isomerase A	√	
SPD_0822	**proB**	**glutamate 5-kinase**		**√**
SPD_0823	proA	gamma-glutamyl phosphate reductase		√
SPD_0824	proC	pyrroline-5-carboxylate reductase		√
SPD_0907	hemK	HemK protein	√	
SPD_0994	ribF	riboflavin biosynthesis protein RibF	√	
SPD_1087	fhs	formate--tetrahydrofolate ligase		√
SPD_1090		membrane protein, putative		√
SPD_1098		**amino acid ABC transporter, amino acid-binding**	**√**	**√**
SPD_1099		amino acid ABC transporter, ATP-binding protein		√
SPD_1130	licD2	phosphotransferase LicD2		√
SPD_1293		acetyltransferase, GNAT family protein		√
SPD_1309	pgdA	peptidoglycan GlcNAc deacetylase		√
SPD_1333		conserved hypothetical protein		√
SPD_1354		conserved hypothetical protein	√	
SPD_1414		**oxalate:formate antiporter**	**√**	**√**
SPD_1468		phosphoglycerate mutase	√	
SPD_1782	ksgA	dimethyladenosine transferase	√	
SPD_1923		2,3,4,5-tetrahydropyridine-2-carboxylate N-succinyltransferase,	√	
SPD_2047	**cbiO1**	**cobalt ABC transporter, ATP-binding protein CbiO1**	**√**	**√**
SPD_2048	cbiO2	cobalt ABC transporter, ATP-binding protein CbiO2		√
Total			**17**	**23**

Impaired Bacterial Metabolism Selectively Reduces Fitness *In Vitro*

To assess the differential fitness of genes predicted by Tn-seq, we generated 5 single-gene deletion bacterial mutants (D39Δ*cbiO1*, D39Δ*purD*, D39Δ*1414*, D39Δ*1098*, and D39Δ*proB*) (Table 1, Fig 1, and Tables S2-S3). *In vitro* growth of the knockouts in ThyB was unaffected by the gene deletion with the exception of D39Δ*cbiO1*, which was significantly attenuated from 3 h to 8 h (Fig 2A). Consistent with this finding was the observed morphological changes of D39Δ*cbiO1*, which tended to be smaller and grow slower than wild-type (WT) D39 on blood agar plates. Interestingly, D39Δ*cbiO1* was the only bacterial strain that had not lysed after 24 h in culture (Fig 2A). We examined decay kinetics in PBS to assess the fitness of knockout bacteria under conditions of metabolic starvation. The decay rates of knockout bacteria were similar to that of WT D39 with the exception of D39Δ*1098 and* D39Δ*cbiO1* (Fig 2B). D39Δ*1098* decayed rapidly and became undetectable 3 h before WT D39 ($p=0.01$) while D39Δ*cbiO1* decayed more slowly and survived in culture 3 h longer than WT D39 ($p<0.01$) (Fig 2B). Although the decay rate of D39Δ*1414* was similar to WT D39 ($p=0.25$), the rate increased at 9 h of culture and bacteria became undetectable 3 h earlier than WT D39 (Fig 2B). Growth of each of the knockout bacteria was reconstituted following metabolic starvation when cultures were supplemented with lung homogenate supernatants (s/n) from mock- or IAV-infected mice (Fig S1).

To assess the requirement of influenza virus-mediators for bacterial growth of the knockouts, we examined growth kinetics in lung homogenate s/n from naïve or IAV-infected mice (75 $TCID_{50}$ PR8, 7 d pi) (Fig 2C-D). In both naïve and IAV-infected lungs, knockout bacteria titers were only slightly lower than WT D39 ($p>0.05$) after 6 hours of growth (Fig 2C-D). Specifically, after 6 h of growth in naïve lung s/n, WT D39 titers were 8.7 $\log_{10}$ CFU/ml, while titers of knockout bacteria ranged from ~7.0 to 8.0 $\log_{10}$ CFU/ml (all $p>0.05$) (Fig 2C). In lung s/n from IAV-infected mice,

titers of WT D39 were 8.3 $\log_{10}$ CFU/ml, while titers of knockout bacteria ranged from ~6.7 to 8.0 $\log_{10}$ CFU/ml (all $p>0.05$) (Fig 2D).

Impaired Bacterial Metabolism Protects Against Virulence *In vivo*

Reduced Mortality

Mice were infected with 75 $TCID_{50}$ PR8 or mock control (PBS) followed by 1e6 CFU WT D39 or one of the knockouts at 7 d pi to examine the effect of gene deletion on pathogenicity (Fig 3, Table S4). In PBS- and IAV-infected animals, infection with WT D39 resulted in 100% mortality by 72 h pbi and 48 pbi, respectively. In PBS-infected animals, mortality was reduced by 90-100% in 4 out of 5 knockouts and by 40% with D39Δ*proB*, compared to WT D39 (all $p<0.01$) (Fig 3C, Table S4). Correspondingly, weight loss at 48 h pbi with each knockout was significantly reduced compared to WT D39 ($p<0.05$) (Fig 3A). In IAV-infected animals, mortality was reduced by 40-90% in 4 out of 5 knockouts compared to WT D39 (all $p<0.01$) (Fig 3D, Table S4). Coinfection with D39Δ*proB* resulted in 100% mortality; however, the mean survival time was lengthened by 5 d ($p<0.01$) (Fig 3D, Table S4). In IAV-infected animals, weight loss was not significantly reduced compared to WT D39 ($p>0.05$) (Fig 3B).

Reduced Bacteria in the Lung and Blood

The growth capabilities of knockout bacteria observed in lung supplemented cultures *in vitro* (Fig 2C-D) were mirrored in *in vivo* growth kinetics (Fig 4A-B). Specifically, in both PBS- and IAV-infected animals, titers were lower than WT D39 in the lungs for each knockout bacteria at 4 h pbi ($p<0.01$) (Fig 4A-B, Table S4). By 24 h pbi, titers were similar to WT D39 in both the lungs and blood of PBS-infected animals ($p>0.05$) (Fig 4A, Fig 4C, and Table S4). However, at 24 h pbi in IAV-infected animals, each of the knockout bacteria grew to significantly lower titers than WT D39 in both the lungs ($p<0.05$) and blood ($p<0.01$) (Fig 4B, Fig 4D, and Table S4). Of note, D39Δ*cbiO1*

was not detected in the lungs of mock infected animals at 24 h pbi and was measured at low levels in 2 out of 5 mice at 48 h pbi and 1 out of 5 mice at 72 h pbi (Fig 4A). Despite attenuated growth in the lungs and reduced bacteremia at 24 h pbi, bacterial loads for each knockout remained high in the lungs and blood of coinfected animals at 24 h, 48 h, and 72 h pbi (Fig 4B, Fig 4D, and Table S4).

Similar Viral Load Kinetics

Similar to previous studies, viral loads rebounded following coinfection with each bacterial strain (Fig 4E, Table S4). Although the viral loads were not significantly different between the knockouts and WT D39 ($p>0.05$), there were some kinetic differences amongst the knockouts. The viral rebound during coinfection with D39Δ*purD* and D39Δ*1098* was delayed and the peak viral rebound in D39Δ*1098* was slightly lower compared to coinfection with the other knockouts and WT D39 (Fig 4E, Table S4).

Altered Cytokine and Chemokine Responses

Because there was marked improvement in morbidity and mortality despite high pathogen burdens, we examined how infection with each of the knockouts affected cytokine and chemokine dynamics in the lungs (Fig 5, Fig S2-S4). In IAV-infected animals, there were significantly reduced levels of IFN-α, IFN-β, IL-6, KC, MIP-1β and GM-CSF at 24 h pbi during coinfection with knockout bacteria compared to WT D39 ($p<0.05$), with the exception of IFN-α during D39Δ*1414* ($p=0.95$) and D39Δ*purD* ($p=0.17$) coinfection (Fig 5, Fig S2-S4). IFN-α, IL-6, KC, and MIP-1β were not lower at 24 h pbi ($p>0.05$) with each of the knockout bacteria in PBS-infected animals (Fig 5, Fig S2-S4). IL-1α , IL-1β, MIP-1α, and TNF-α were reduced in both PBS- and IAV-infected animals at 24 h pbi with each knockout bacteria compared to WT D39 ($p<0.05$), except for D39Δ*purD* in PBS-infected animals ($p>0.05$) (Fig 5, Fig S2-S4). Interestingly, at 4 h pbi in IAV-infected animals,

IFN-α was elevated in D39Δ*1414*, D39Δ*cbiO1*, D39Δ*purD*, and D39Δ*1098* coinfections ($p<0.01$) and IFN-β was elevated in D39Δ*cbiO1* coinfection ($p<0.01$) (Fig 5, Fig S2J and L). Minimal changes were detected in amounts of MCP-1, RANTES, IL-2, IFN-γ, IL-10, IL-12(p40), and IL-12(p70) during coinfection with any of the knockouts compared to WT D39 (Fig 5, Fig S3-S4).

Altered Cellular Responses

In accordance with the changes detected in pulmonary cytokines and chemokines, infection with knockout bacteria altered dynamics of select immune cells in the lungs (Fig 6 and Figs S5-S6). Most notably, in IAV-infected animals, neutrophils ($Ly6G^{hi}$) were significantly reduced at 4 h pbi during coinfection with D39Δ*1098* ($p<0.01$) and D39Δ*proB* ($p<0.05$), and at 24 h pbi during coinfection with D39Δ*1414*, D39Δ*cbiO1*, D39Δ*purD*, and D39Δ*proB* ($p<0.05$) (Fig 6B) compared to coinfection with WT D39. Inflammatory macrophages (IMΦs; $Ly6G^{-}$, $CD11c^{hi}$, $F4/80^{hi}$, $CD11b^{+}$) were reduced at 4 h pbi during coinfection with D39Δ*1414*, D39Δ*purD*, D39Δ*1098*, and D39Δ*proB* ($p<0.05$) (Fig 6D). Coinfection with D39Δ*cbiO1* did not lead to reduced IMΦs at 4 h pbi ($p=0.14$), but did enduce a significant increase in IMΦs at 24 h pbi ($p<0.01$) (Fig 6D). In PBS-infected animals, neutrophils and IMΦs were not significantly different in any of the knockouts compared to WT D39 at 4 h pbi ($p>0.05$) (Fig 6A, Fig 6C). At 24 h pbi, only infection with D39Δ*purD* ($p<0.05$) and D39Δ*cbiO1* ($p<0.05$) resulted in altered neutrophils and IMΦs, respectively (Fig 6A, Fig 6C). There were minimal differences in the extent of AMΦ depletion ($Ly6G^{-}$, $CD11c^{hi}$, $F4/80^{hi}$, $CD11b^{-}$) (Fig 6E-F) or T cell subset (Fig S6I-L) in PBS- and IAV-infected animals with knockout bacteria compared to WT D39.

Reduced Pathology and Altered Neutrophil Phenotype

Performing hematoxylin and eosin (HE) staining on the lungs of coinfected mice at 24 h pbi revealed extensive pulmonary consolidation in the lungs of mice coinfected with WT D39, as

characterized by thickened septa and alveoli filled with a mixture of neutrophils, free bacteria, and proteinaceous exudates (Fig 7A). This was dramatically reduced during coinfection with D39Δ*proB,* D39Δ*1098, and* D39Δ1414 and absent in D39Δ*cbiO1* and D39Δ*purD* coinfection (Fig 7A). Immunohistochemical (IHC) staining showed that there was less bacterial antigen at 24 h pbi during coinfection with each of the knockout bacteria compared to WT D39 (Fig 7B), which mirrored the pulmonary bacterial loads (Fig 4B). In WT D39 coinfected mice, there was intracellular and extracellular bacterial antigen present throughout influenza-lesioned areas, including pervascular connective tissues, consolidated alveolar parenchyma, and the central hypocellular area of resolving lesions. Bacterial antigen was not detected in the resolving influenza lesions with any of the knockout bacteria, except for D39Δ*1098* where few bacteria or antigen-positive macrophages were present. IHC staining also showed drastic neutrophil infiltration in WT D39 coinfection, and the resolving influenza lesions were surrounded by sharply demarcated hypercellular bands consisting of intact and degenerating neutrophils (Fig 7C). Neutrophils were reduced, although still abundant, in lungs of animals coinfected with D39Δ*proB,* D39Δ*purD*, D39Δ*1098*. However, all cells were intact and occured in indistinct bands surrounding influenza lesions, clustered within alveoli peripheral to influenza lesions, or scattered throughout inflamed areas (Fig 7C). Animals coinfected with D39Δ*1414* and D39Δ*cbiO1* had the least neutrophils, which were morphologically intact and scattered throughout inflamed areas (Fig 7C). Neutrophils were rare or absent within the resolving influenza lesions in animals coinfected with each of the knockout bacteria .

Discussion

Pathogenicity during influenza-pneumococcal coinfection is influenced by several factors, including the viral and bacterial strain and doses, and the strength of the inflammatory response (Reviewed in references 11-16). Although viral and bacterial strain variability does influence

coinfection severity (8-10, 51), how specific genetic factors contribute to pathogenicity has been relatively unexplored. Pneumococci, in particular, are highly adaptable and alter gene expression, protein production and modification, and metabolic functions to adjust to multiple host niches during infection (22, 52-66). In addition, its distributed genome is due to frequent recombination and horizontal gene transfer events (52), which facilitate its versatility. This is unlike the strategies employed by other bacteria like *Staphylococcus aureus*, another prominent influenza-coinfecting agent (1, 4, 5, 8, 67), where approximately 70% of the genome is conserved (68, 69). Given the genomic diversity and flexibility within pneumococcal strains, we sought to establish the genetic contribution to clinical phenotype of secondary bacterial pneumonia.

Here, using Tn-Seq as an unbiased approach to identify bacterial genes critical to pneumococcal survival in the IAV-infected host, we pinpointed 32 genes that alter bacterial fitness in a time-dependent manner (Table 1, Fig 1). By generating 5 single-gene deletion mutants of D39, we established that bacteria with altered metabolic capacities induce dramatically altered immune responses in IAV-infected hosts (Fig 5-7, S2-4, and S6). This reduction in immune activation, immune cell infiltration, and pulmonary damage, also occurred in a time-dependant manner (Fig 5-7, S2-4, and S6). These findings are provocative and consistent with other studies that have discovered time-dependent mechanisms during influenza-pneumococcal coinfection (29, 30, 70). Of note, none of the genes critical for growth in IAV-infected hosts were known bacterial virulence factors (45-47). This is likely because those factors affect disease equally regardless of viral infection status. The identified genes are mostly involved in bacterial metabolism, which supports findings that the metabolome of the lung is altered during influenza virus infection (71-74). Indeed, altered metabolic regulation has been observed during murine influenza virus infection (71, 72), *in vitro* influenza virus infection of primary human bronchotracheal epithelial (HBAE) cells (73, 74), and in pediatric patients infected with influenza virus (73). However, even with the knowledge that influenza virus induces metabolic changes and that pneumococci modulate metabolic

pathways under host-specific pressures (49, 75), the specific collection of genes identified here was not intuitive.

Some common features did emerge when comparing our results with other studies. For example, adaptations specific to purine biosynthesis were previously found to occur in *Haemophilus influenzae* within influenza-infected hosts (48) and in pneumococci within hosts with sickle-cell disease (49). Here, eight genes with roles in purine metabolism were identified in our screen, including SPD0058 (*purD*) (76-78) (Table 1, Fig 1). This could indicate a common mechanism for bacterial adaptation in inflammatory environments. Specifically, in the influenza-infected host, purine biosynthesis is upregulated (71) and purine analogs can be used to reduce disease severity (e.g., by the antiviral T-705(79, 80)). However, the intermediates of purine biosynthesis become depleted following bacterial infection (48), rendering purine biosynthesis a critical function for coinfecting bacteria (48, 49). D39Δ*purD* would rely heavily on purine scavenging, which could alter host immune cell function through competition for environmentally available purines and contribute to decreased lethality (Fig 3D) and immunopathology (Fig 7A) compared to WT bacteria in IAV-infected hosts.

Several of the genes identified here act in glutamate/glutamine biosynthesis, which suggests that these changes have a key role during influenza-pneumococcal coinfection. For example, the locus pinpointed as the main ABC glutamine/glutamate transporter in pneumococci is SPD1098/1099(81, 82), which was identified in our screen. Deletion of SPD1098 had the most profound improval on survival (90%) in coinfected animals (Fig 3D). In addition, SPD0822/0823 (*proB/A*), which act in proline biosynthesis, were identified in the screen and are downstream of glutamate metabolism (76-78). Deletion of SPD0822 (*proB*) did not lower coinfection pathogenicity, but did alter the time course of disease and delay mortality (Fig 3D). Interestingly, D39Δ*1098* and D39Δ*proB* led to reduced neutrophils and iMΦ in influenza-infected hosts early in

the infection (4 h pbi), but resulted in no changes in naïve hosts (Fig 6). In general, glutamine is utilized at a high rate by immune cells and is needed for optimal function of macrophages and neutrophils (83-88). In addition, pulmonary cells have increased dependence on glutamine during influenza virus infection (73). Thus, during influenza-pneumococcal coinfection, pneumococci and/or influenza-infected cells are in competition for glutamine with host immune cells. Here, altered competition for limited enivonmentally available glutamine may have reduced neutrophil infiltration and dysfunction, resulting in less morbidity and mortality in IAV-infected hosts (Fig 3D and Fig 5-7).

The function of some of the genes identified in our screen, including three other ABC transporters (e.g., SPD2047/2048 (*cbiO1/2*) and SPD1414), are less understood. In general, ABC transporters are important for pneumococcal virulence (52, 60, 89-92). Thus, it was expected that deleting these genes would reduce the growth capacity of D39. Futher understanding the specific impacts of each knockout mutant may provide insight into other respiratory changes that occur during influenza virus infection. For example, bacteria lacking the cbiO locus (putative cobalt transporter), previously identified by microarray analysis as necessary for pneumococcal pathogenicity (62), grow to significantly higher titers in IAV-infected animals than naïve animals (Fig 4A-D), suggesting that cobalt metabolism is modified by influenza virus infection. The TIGR4 analog of the oxalate/formate antiporter SPD1414 (SP1587) is important for bacterial survival in the lungs and blood (60, 93), cerebral spinal fluid (60), and nasopharynx (93). Here, deletion of SPD1414 did not result in lower bacteremia in naïve animals (Fig 4C), but did reduce bacteremia, neutrophil infiltration, and pulmonary damage in IAV-infected hosts the most dramatically (Fig 4D, Fig 6-7). It is unclear how each of these alterations contributed to the improved survival in IAV-infected hosts (Fig 3D).

Mortality during influenza-pneumococcal coinfection is typically associated with an exuberant immune response coupled with high pathogen loads in the lung and the blood (14-16, 34, 94-96). However, reduced inflammation can lessen severity even with sustained bacterial loads (36). Here, the attenuated growth of each of the knockout bacteria in IAV-infected animals was significant (0.8-2.1 $\log_{10}$ reduction compared to WT D39), but insufficient to account for the extreme reductions in mortality (up to 90%) (Fig 3D, Fig 4, Table S4). AMΦ, which dictate the initial pneumococcal invasion and growth kinetics during IAV infection (28-31), are not different during coinfection with each knockout bacteria compared to WT D39 (Fig 6F), except for D39Δ*proB* at 4 h pbi and D39Δ*purD* at 24h pbi. This suggests that the observed differences in immune responses and disease outcome are not driven by the differences in bacterial loads. Reduced inflammation, specifically lowered type I IFNs (Fig 5, Fig S2J and L) during coinfection with knockout bacteria may have improved neutrophil function (32, 34, 35, 70, 97-100) and reduced epithelial cell death and lung permeability (101) and, thus, reduced coinfection pathogenicity (Fig 3D, Fig 5, and Fig 7). Moreover, reduced neutrophil infiltration and degredation (Fig 6B, Fig 7C) likely mitigated the damaging cytokine storm that is typically associated with IAV-pneumococcal pneumonia (Reviewed in references 12-16, 21, 43).

Here, there were not significant differences in viral load rebounds (Fig 4E) or contraction of the pulmonary $CD8^+$ T cells (102) (Fig S6L) during coinfection with knockout bacteria despite reduced lung pathology, hypercytokinemia, and lethality (Fig 3D, Fig 5, and Fig 7). These results support our previous findings that the mechanisms underlying rapid bacterial growth are independent from those that influence the post-bacterial viral rebound and pathogenicity (29, 30). A direct correlation between survival and any single host immune response in the early stages of coinfection (0-24 h pbi) was not readily apparent. It is possible that unmeasured components and/or a cumulative effect influences lethality at later time points. These studies underscore the independent nature

of pathogen growth and pathogenicity and illuminate the difficulty in reducing coinfection pathogenicity to a single variable.

Understanding how bacterial adaptations influence the development of pneumonia during influenza virus infections is important to effectively combat the disease. Here, we provide insight into the contribution of specific pneumococcal genes and to the regulatory host-pathogen dynamics that arise during the coinfection. Our findings highlight the critical role of influenza-mediated metabolomic shifts in inducing immune defects and promoting bacterial infection, and suggest that targeting a single pneumococcal gene or metabolite could be an effective intervention to abrogate bacterial pneumonia during influenza infection. Further dissecting bacterial adaptation may identify additional therapeutic targets that could be used to prevent or treat post-influenza bacterial infections.

Materials and Methods

Ethics Statement All experimental procedures were performed under protocol O2A-020 approved by the Animal Care and Use Committee at St. Jude Children's Research Hospital under relevant institutional and American Veterinary Medical Association (AVMA) guidelines and were performed in a biosafety level 2 facility that is accredited by the American Association for Laboratory Animal Science (AALAS).

Tn-Seq Plasmid DNA harboring *magellan6,* a derivative of the Himar1 Mariner transposon, was purified from *E. coli* with the Qiagen mini plasmid preparation kit (Qiagen). Pneumococcal DNA was isolated by phenol/chloroform extraction and ethanol precipitation from an exponentially growing culture in ThyB media (30 mg/ml Todd-Hewitt Broth powder and 0.2 mg/ml yeast). *In vitro, magellan6* transposition reactions were carried out with purified MarC9 transposase, 1 µg

of pneumococcal target DNA and 1 µg of *magellan6* plasmid DNA. Reactions were incubated for 1 h at 30°C, inactivated for 20 min at 72°C, ethanol precipitated and resuspended in gap repair buffer [50 mM Tris (pH 7.8), 10 mM $MgCl_2$, 1 mM DTT, 100 nM dNTPs and 50 ng BSA]. Repair of transposition product gaps was performed with *E. coli* DNA ligase overnight at 16°C. Repaired transposition products were transformed into naturally competent pneumococcal strain D39. The following day, colonies were scraped off tryptic soy-agar (TSA) plates supplemented with 3% sheep erythrocytes and 200 mg/ml spectinomycin (TSA-Spec), pooled into libraries of approximately 50,000 transformants/library, split up into multiple starter cultures and stored at -20°C.

Mice Adult (6 week old) female BALB/cJ mice were obtained from Jackson Laboratories (Bar Harbor, ME). Mice were housed in groups of 5 in high-temperature 31.2cm x 23.5cm x 15.2cm polycarbonate cages with isolator lids. Rooms used for housing animals were maintained on a 12:12-hour light:dark cycle at 22 ± 2°C with 50% humidity in the biosafety level 2 facility at St. Jude Children's Research Hospital (Memphis, TN). Prior to inclusion in the experiments, mice were allowed at least 7 days to acclimate to the animal facility such that they were 7 weeks old at the time of infection. Laboratory Autoclavable Rodent Diet (PMI Nutrition International, St. Louis, MO) and autoclaved water were available ad libitum. All experiments were performed under an approved protocol and in accordance with the guidelines set forth by the Animal Care and Use Committee at St. Jude Children's Research Hospital.

Infectious Agents All experiments were done using the mouse adapted influenza A/Puerto Rico/8/34 (H1N1) (PR8) and type 2 pneumococcal strain D39 variants. To generate the D39 knockout mutants, genomic DNA was isolated by phenol:chloroform extraction from an exponentially growing culture of WT D39 in ThyB media following genomic lysis (37°C, 10 min,

(25 mM Tris-HCl, 10 mM EDTA, 50 mM glucose, 0.1 mg/ml RNase, 5 mg/ml deoxycholic acid, 5 mg/ml sodium dodecyl sulfate, and 8 u Proteinase K in molecular grade dH_2O)). The same technique was used to isolate genomic DNA from *S. pneumoniae* (T4ΔHtrA) containing the erythromycin (ERM) resistance cassette. These were used as template DNA for gene SOEing PCR (103, 104). In brief, regions flanking the D39 locus targeted for deletion and containing overhangs complementary to the ERM resistance cassette (labeled regions A and B) were generated using the primer sets indicated in Table S2. Regions A, B, and ERM resistance cassette were amplified at the cycle conditions indicated in Table S2 (EasyA PCR kit (Agilent Tech) and BioRad T100 thermal cycler). Products were purified from a 1% agarose gel using the Zymoclean gel DNA recovery kit (Zymo Research). Regions A, B, and ERM resistance cassette were recombined by PCR (TaKaRa PCR kit (Clontech Laboratories)) using the primers and cycle conditions in Table S3. The recombined products were purified from gel as above and transformed into D39. Transformed bacteria were selected after overnight growth on TSA plates containing 1 μg/ml ERM (TSA-ERM). Infection stocks were grown in ThyB media containing 1 μg/ml ERM, and frozen in 12% glycerol stocks for animal infections. ERM resistance cassette insertion and target locus deletion were confirmed by PCR with the primer sets in Table S3.

Infection Experiments The viral infectious dose ($TCID_{50}$) was determined by interpolation using the method of Reed and Muench (105) using serial dilutions of virus on Madin-Darby canine kidney (MDCK) cells. The bacterial infectious dose (CFU) was determined by using serial dilutions on TSA (WT), TSA-ERM (knockouts), or TSA-Spec (Tn-seq) plates. Inocula were diluted in sterile PBS and administered intranasally to groups of 5 (for kinetics) or 10 (for bacteria collection and survival) mice lightly anesthetized with 2.5% inhaled isoflurane (Baxter, Deerfield, IL) in a total volume of 100 μl (50 μl per nostril). Mice were inoculated with either PBS or 75 $TCID_{50}$ PR8 at day 0 then with the indicated CFU of D39 or knockout mutant (in 100 μl), 7 days later. Animals

were weighed at the onset of infection and each subsequent day to monitor illness and mortality. Mice were euthanized if they became moribund or lost 30% of their starting body weight.

Lung and Blood Harvest for Bacteria Sequencing Mice were euthanized by CO_2 asphyxiation. Lungs were perfused with 10 ml PBS, aseptically harvested, washed three times in PBS, and placed on ice in 500 µl PBS. The post-perfusion fluid (mixture of blood and PBS) was plated immediately on TSA-Spec plates (150 µl/plate). The lungs were then enzyme digested with collagenase (1 mg/ml, Sigma), and physically homogenized by syringe plunger against a 40µm cell strainer. Cell suspensions were centrifuged at 4°C, 500xg for 7 min and the supernatant was plated on TSA-spec plates (100 µl/plate).

Bacterial Collection for Sequencing Following infection, 500 µl of the inoculum was plated on TSA-Spec plates (100 µl/plate). Bacteria were collected from infected mice at 12 h pbi and 24 h pbi and plated on TSA-Spec plates (500 µl; 100 µl/plate). Later time points could not be examined due to insufficient numbers of live mice at 48 h pbi. For each mouse, ~200 µl blood was plated upon harvest, and ~500 µl of lung supernatant was plated following lung digestion (see above). Bacteria were incubated for 12 h at 37°C then collected in ThyB media and centrifuged at 4°C, 500xg for 10 min. The media supernatant was removed and the pellets were stored at -20°C.

Bacterial Fitness By Tn-Seq Bacterial gene identification by Tn-Seq was performed as described previously (49, 50, 93). The samples at each of the three time points (pre-selection (inoculum, t_1) and post-selection (after infection, 12 h (t_2) or 24 h (t_3) pbi), were sequenced in rapid run mode on an Illumina HiSeq 2000. For each insertion, the fitness *Wi*, was calculated by comparing the fold expansion of the mutant relative to the rest of the population with the following equation (106).

$$W_i = \frac{\ln\ [N_i(t_{2,3})d/N_i(t_1)]}{\ln\ [(1 - N_i(t_{2,3}))d/(1 - N_i(t_{2,3}))]}$$

where the mutant frequency at time 0 and harvest are $N_i(t_1)$ and $N_i(t_{2,3})$, respectively. The expansion factor (d) accounts for bacterial growth during library selection. Additional details of the method are included in the Supplementary Information.

Lung Harvest for *In vitro* Kinetics Mice were euthanized by CO_2 asphyxiation. Lungs were aseptically harvested, washed three times in PBS, and placed in 500 µl PBS. Lungs were homogenized (Omni TH-01 with 5mm flat blade) and centrifuged at 4°C, 500xg for 7 min. Bacteria were grown at 37ºC in 1.0 ml lung supernatants or in 1.0 ml PBS. A subset of PBS cultures were supplemented with 0.5 ml lung homogenate supernatant after 5 h of metabolic starvation (Fig S1). At each time point, 50 µl was removed, serially diluted in PBS, and plated on TSA (WT) or TSA-ERM plates. Bacterial titers were normalized to the total volume.

Lung Harvest for *In Vivo* Kinetics Mice were euthanized by CO_2 asphyxiation. Lungs were aseptically harvested, washed three times in PBS, and placed in 500 µl PBS. Lungs were enzyme digested with collagenase (1 mg/ml, Sigma C0130), and physically homogenized by syringe plunger against a 40 µm cell strainer. Cell suspensions were centrifuged at 4°C, 500xg for 7 min and the supernatants were used to determine the viral titers, bacterial titers, cytokine/chemokine levels (5 mice/group). Following red blood cell lysis, cells were washed in MACS buffer (PBS, 0.1 M EDTA, 0.01 M HEPES, 5 mM EDTA and 5% heat-inactivated FBS), counted with trypan blue exclusion using a Cell Countess System (Invitrogen, Grand Island, NY), and prepared for flow cytometric analysis as described below.

Lung and Blood Titers For each mouse, viral titers were obtained using serial dilutions on MDCK monolayers, and bacterial lung titers and bacterial blood titers were obtained using serial dilutions on TSA (WT) or TSA-ERM (knockouts) plates, respectively.

Cytokines Cytokines and chemokines were measured in lung supernatant by luminex (GM-CSF, IFN-γ, IL-1α, IL-1β, IL-2, IL-6, IL-10, IL-12(p40), IL-12(p70), KC, MCP-1, MIP-1α, MIP-1β, RANTES, and TNF-α) and ELISA (IFN-α,β). Prior to use, cell debris and aggregates were removed from lung supernatants by centrifugation at 4°C, 400xg. Milliplex magnetic bead cytokine/chemokine plates (Millipore) were prepared according to manufacturer's instructions. Analysis was done using a BioRad BioPlex (HTF System) and Luminex xPonent software. Concentrations of duplicate samples were determined by construction of a standard curve for each analyte with a weighted 5PL method. ELISAs for IFN-α and IFN-β (PBL Assay Science) were prepared according to the manufacturer's instructions. Plates were read at 450 nm and analyzed using elisaanalysis.com. Mean concentrations of duplicate samples were determined by construction of a standard curve with a 4PL regression. Absolute quantities of each cytokine/chemokine were calculated based on mean concentration of replicate samples normalized to the lung supernatant volume collected during tissue processing.

Flow Cytometric Analysis Flow cytometry (LSRII Fortessa; Becton Dickinson, San Jose, CA) was performed on single cell suspensions after incubation with 200 μl of 1:2 dilution of Fc block (human-γ globulin) on ice for 30 min, followed by surface marker staining with anti-mouse antibodies: CD11c (eFluor450, eBioscience), CD11b (Alexa700, BD Biosciences), Ly6G (PerCp-Cy5.5, Biolegend), Ly6C (APC, eBioscience), F4/80 (PE, eBioscience), CD3e (PE-Cy7, BD Biosciences or BV785, Biolegend), CD4 (PE-Cy5, BD Biosciences), CD8α (BV605, BD Biosciences), DX5 (APC-Cy7, Biolegend or APC-e780, Affymetrix Inc) and MHC-II (FITC,

eBioscience). The data were analyzed using FlowJo 10.4.2 (Tree Star, Ashland, OR) where viable cells were gated from a forward scatter/side scatter plot and singlet inclusion (Fig S5). Following neutrophil exclusion ($Ly6G^{hi}$), macrophages (MΦ) were gated as $CD11c^{hi}F4/80^{hi}$ with alveolar macrophages (AMΦ) sub-gated as $CD11b^{-}$ and inflammatory macrophages (iMΦ) as $CD11b^{+}$. After macrophage exclusion, T cell populations were gated as $CD3e^{+}$. The $CD3e^{+}$ subset was subgated into CD8 T cells ($CD3^{+}CD8^{+}CD4^{-}DX5^{-}$) and CD4 T cells ($CD3^{+}CD8^{-}CD4^{+}DX5^{-}$). From the $CD3e^{-}$ population, natural killer (NK) cells were gated as $CD3^{-}DX5^{+}$ and dendritic cells (DCs) as $CD3^{-}DX5^{-}$. DC were further gated into three subsets of DC; $CD11c^{+}CD11b^{-}$, $CD11c^{+}CD11b^{+}$, and $CD11c^{-}CD11b^{+}$. The expression levels of MHC-II was used to confirm the identities and activation of MΦ and DC subsets. The absolute numbers of cell types were calculated based on viable events analyzed by flow cytometry and normalized to the total number of viable cells per sample.

Histology Mice were euthanized by CO_2 asphyxiation and lungs were inflated *in situ* via tracheal infusion with 10% neutral-buffered formalin solution (NBF; ThermoFisher Scientific, Waltham, MA), followed by continued fixation in NBF for at least 2 weeks before being embedded in paraffin, sectioned at 4 μm, mounted on positively charged glass slides (Superfrost Plus; Thermo Fisher Scientific, Waltham, MA), and dried at 60°C for 20 min. Tissue sections were stained with hematoxylin and eosin (HE) or subjected to immunohistochemical (IHC) staining to detect influenza antigen, pneumococcus, or neutrophils. For detection of these targets, tissue sections underwent antigen retrieval in a prediluted Cell Conditioning Solution (CC1; Cat# 950-124; Ventana Medical Systems, Indianapolis, IN) for 32 min on a Discovery Ultra immunostainer (Ventana Medical Systems, Tucson, AZ). The primary antibodies used in this study included: a polyclonal goat antibody raised against the HA glycoprotein of B/Florida/04/2006 (Yamagata lineage) influenza virus diluted 1:2000 (cat# I7650-05G, US Biologicals, Swampscott, MA); a

rabbit polyclonal antibody to *Streptococcus pneumoniae* diluted 1:1000 (cat# NB100-64502; Novus Biologicals, Littleton, CO); and a rat monoclonal antibody to neutrophils (Ly6G6C) diluted 1:50 (cat# NB600-1387; Novus Biologicals, Littleton, CO). Binding of these primary antibodies was detected using OmniMap anti-Goat (#760-4647), anti-Rabbit (#760-4311), and anti-Rat (#760-4457) HRP (RUO) respectively (Ventana Medical Systems), with DISCOVERY ChromoMap DAB Kit (Ventana Medical Systems) as chromogenic substrate. Stained sections were examined by a pathologist blinded to the experimental group assignments.

Statistical Analysis Significant differences in Kaplan-Meier survival curves were determined using the log rank test. *In vitro* growth/decay rates were analyzed by nonlinear regression of $\log_{10}$ values, and linear slopes were compared by analysis of covariance (ANCOVA). The remainder of statistical analyses were performed on linear values. Unpaired t-tests were done to analyze *in vitro* growth dynamics in ThyB and lung cultures. Analyses of variance (ANOVA) were performed using a Dunnett correction for multiple comparisons (to WT D39) to analyze *in vivo* differences including, lung and blood bacterial loads, viral loads, immune cells, cytokines, or chemokines (GraphPad Prism 7.0c). The confidence interval of significance was set to 95%, and p values less than 0.05 were considered significant.

Contributions

AMS, JAM, and JR conceived the experiments. AMS, AI, CB, and MJ generated the mutant libraries. DR, RC, and TvO completed the sequence analyses. AMS, APS, and LL generated the knockout bacteria and performed *in vitro/in vivo* experiments. AMS, APS, LL, and GH performed the data analysis. AMS and APS wrote the manuscript.

Acknowledgements

This work was supported by NIH grant AI100946 and AI125324 (AMS), PATRIC DBP (AMS, JR, JAM), ALSAC (APS, LCL, SW, RC, AI, CB, PV, DR, MDLJ, JAM, JR), NIH grant R25CA23944 (GH), and NIH grants R01AI110724, U01AI124302, and R21AI117247 (TvO).

Figures

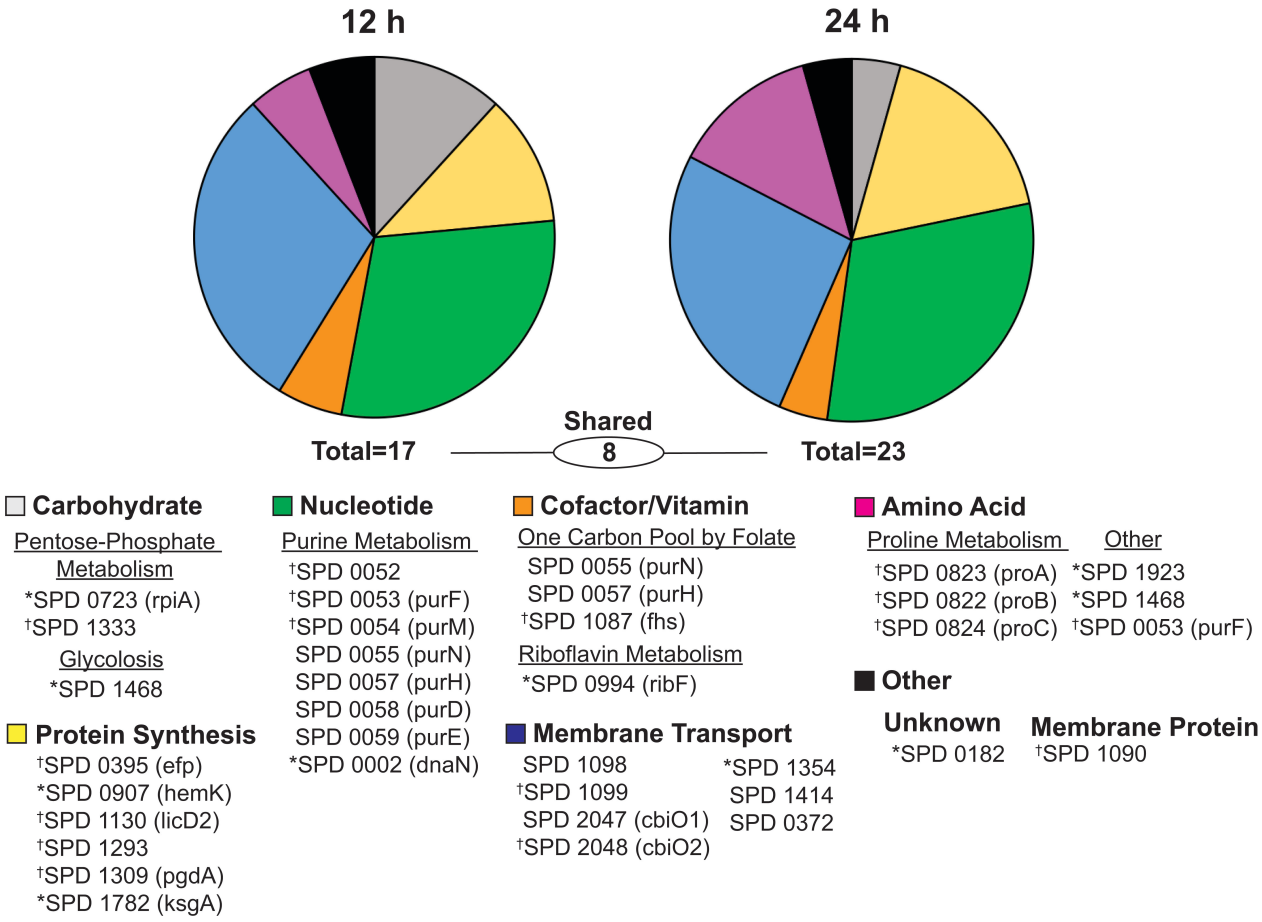

Fig 1: Time-dependent Analysis of Pneumococcal Genes Impacting Fitness During Influenza Virus Coinfection. Functional breakdown of the pneumococcal genes that impact bacterial fitness during coinfection with influenza A virus infection as identified by Tn-Seq. Markers identify genes important at only *12 h pbi (17 total) or only at †24 h pbi (23 total). No marker indicates significance at both time points (8 total).

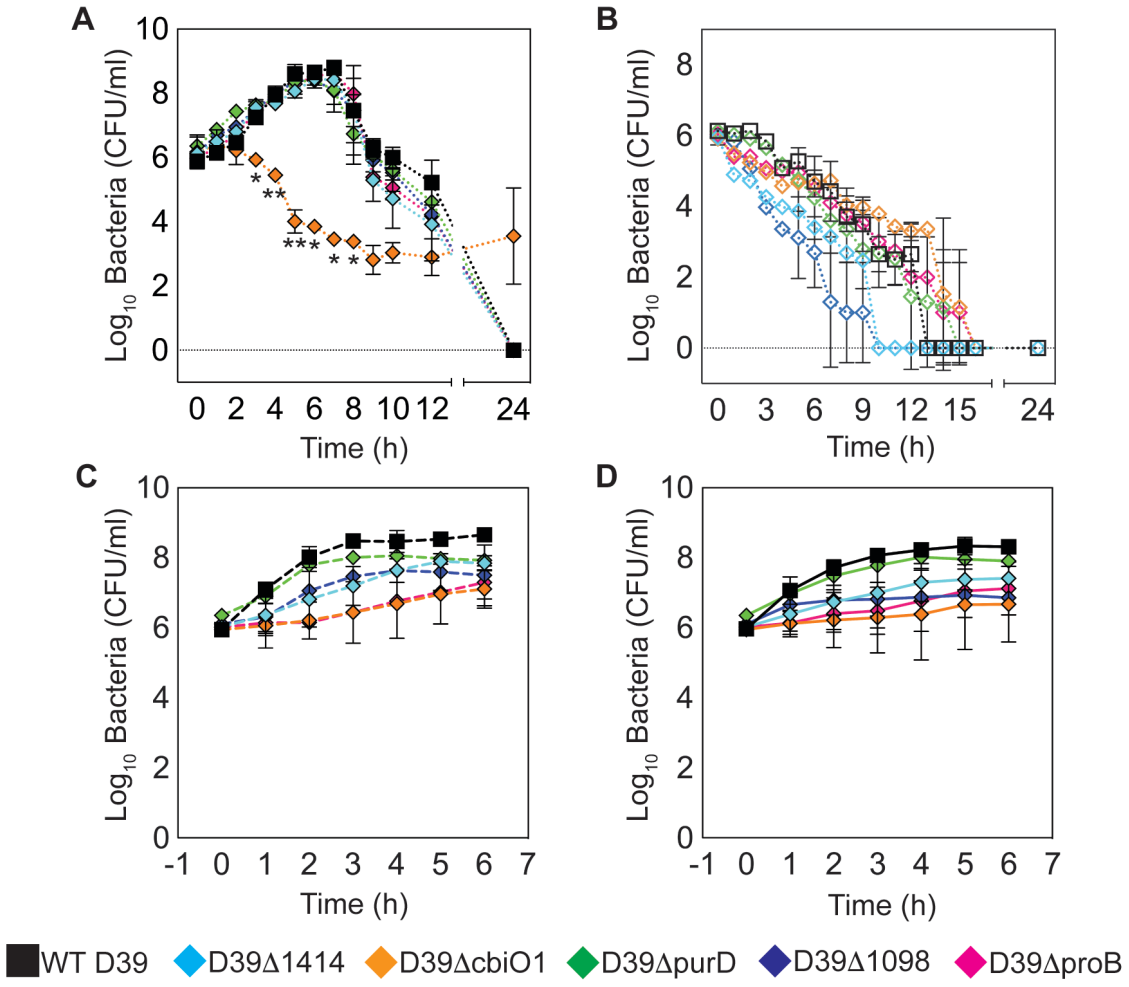

Fig 2: *In vitro* Growth Dynamics of Knockout Bacteria. Bacteria were grown 37°C in 1 ml (A) ThyB, (B) PBS, or (C-D) lung homogenate supernatant. Lung homogenates were obtained from mice infected with PBS (mock) (Panel C) or 75 $TCID_{50}$ PR8 (Panel D) for 7 d. Signficance is indicated as *p<0.05 and **p<0.01 for D39Δ*cbiO1* compared to WT D39 at the indicated time point (Panel A).

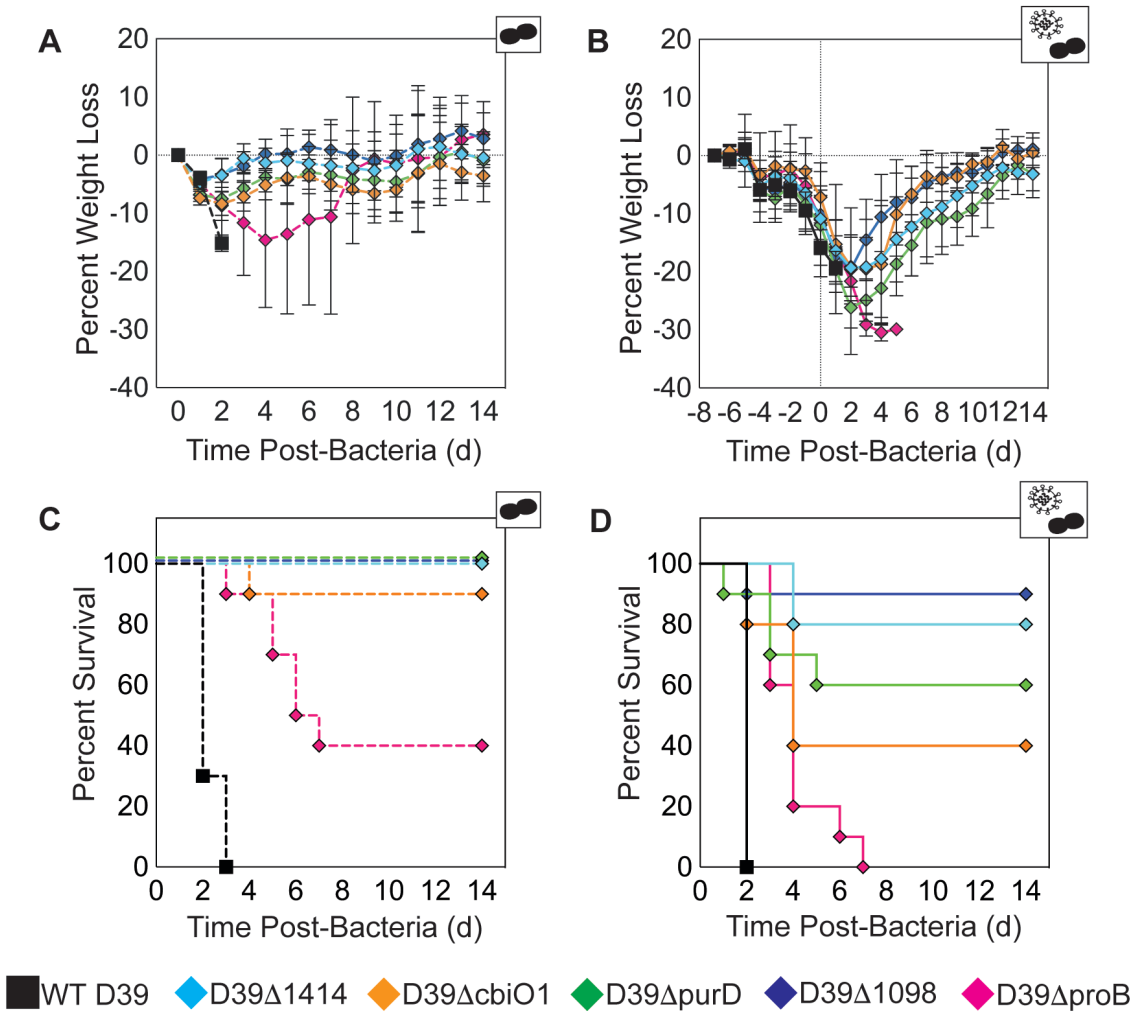

Fig 3: *In vivo* Pathogenicity of Infection with Knockout Bacteria. (A-B) Weight loss (percent loss compared to naïve) of mice infected with PBS (mock) (Panel A) or 75 $TCID_{50}$ PR8 (Panel B) followed 7 days later with 10^6 CFU of the indicated bacteria. (C-D) Kaplan-Meier survival curves of mice infected with PBS (mock) (Panel C) or 75 $TCID_{50}$ PR8 (Panel D) followed 7 days later with 10^6 CFU of the indicated bacteria. Survival curves are significantly different ($p<0.01$) in PBS (mock) (Panel C) and 75 $TCID_{50}$ PR8 (Panel D) animals infected with each of the knockout bacteria compared to WT D39. Differences in Kaplan-Meier survival curves are detailed in Supplementary Information Table S4. Cartoons indicating infection status of study group (bacteria alone or virus plus bacteria) are in the upper right corner of each graph.

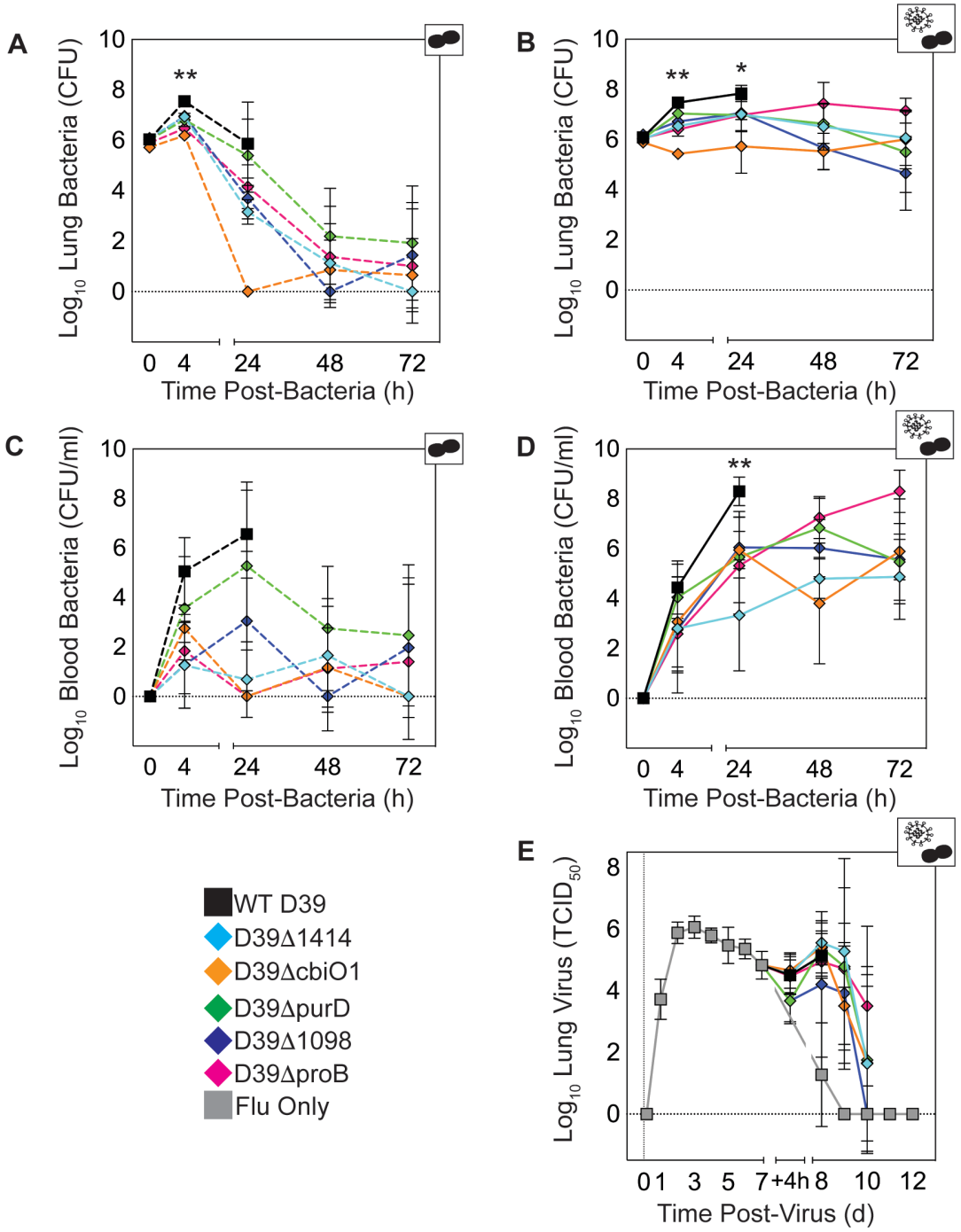

Fig 4: Viral and Bacterial Titer Kinetics. Lung bacterial titers (A-B), blood bacterial titers (C-D) and lung viral titers (E) from mice infected with PBS (mock) (dashed lines; Panels A, C) or 75 $TCID_{50}$ PR8 (solid lines; Panels B, D, E) followed 7 d later with 10^6 CFU of the indicated bacteria. Cartoons indicating infection status of study group (bacteria alone or virus plus bacteria) are in the upper right corner of each graph. Signficance is indicated as *p<0.05 and **p<0.01 for each of the knockout bacteria compared to WT D39 at the indicated time point. The log_{10} change in pathogen loads between each knockout bacteria and WT D39, and analysis of variance results are summarized in Supplementary Information Table S4.

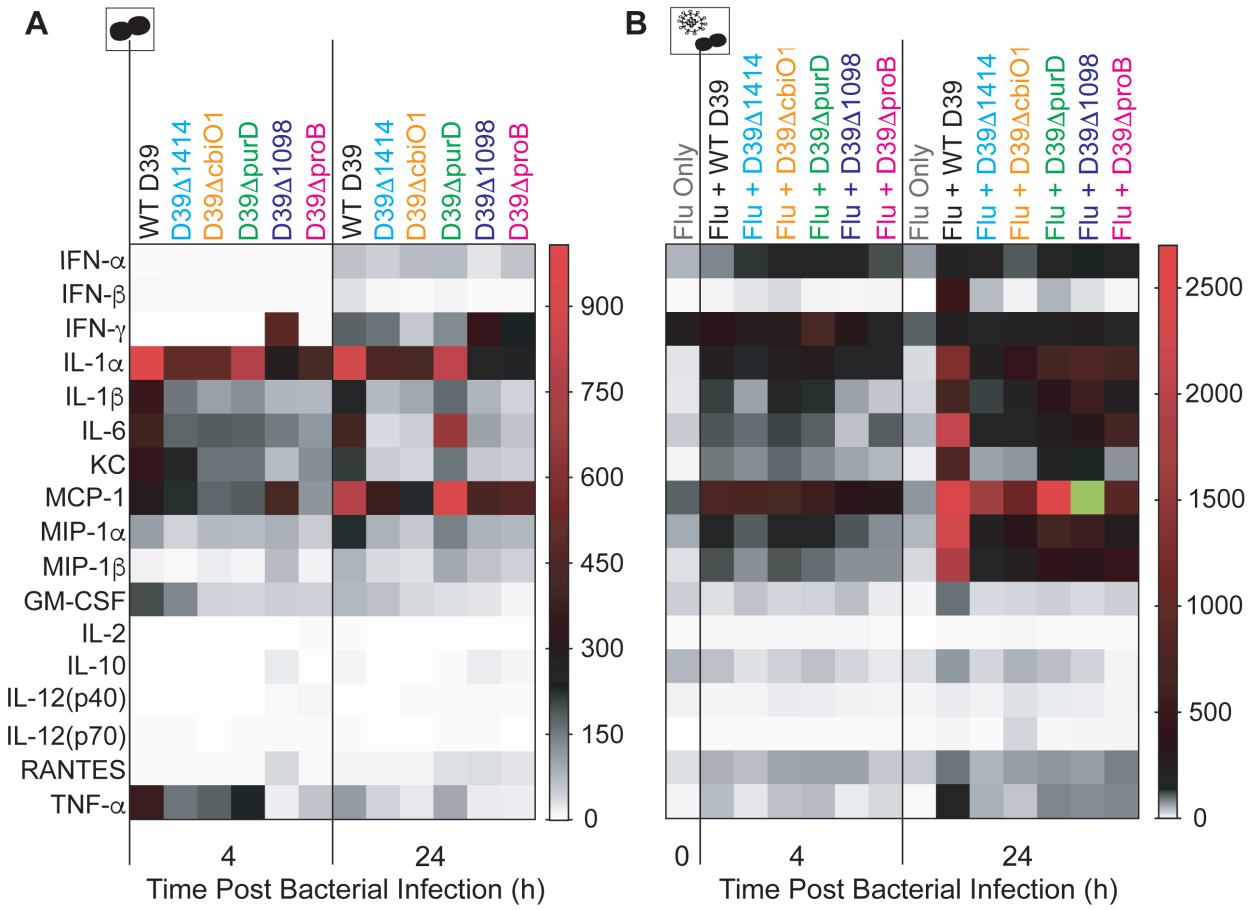

Fig 5: Heat Map of Cytokine and Chemokine Changes. Fold change in the average values of the indicated cytokine/chemokine compared to naïve at 4 h and 24 h pbi from lungs of mice infected with PBS (mock) (A) or 75 $TCID_{50}$ PR8 (B) followed 7 d later with 10^6 CFU of the indicated bacteria. Green square is ouside of heat map range and indicates a 4021 fold change. Cartoons indicating infection status of study group (bacteria alone or virus plus bacteria) are in the upper left corner of each plot. Plots depicting absolute log_{10} picograms (pg) of measured cytokines and chemokines are shown in Fig S2-S4.

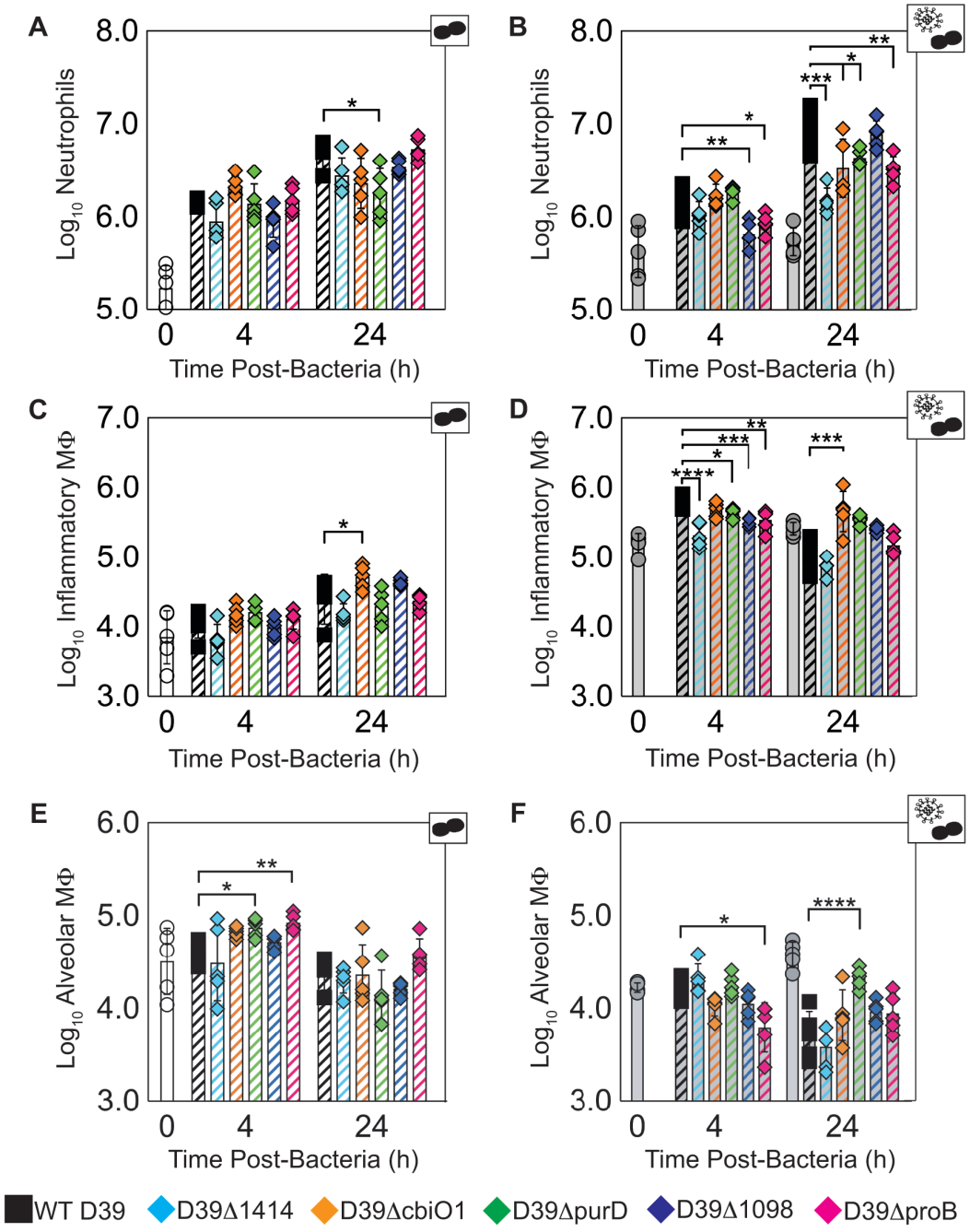

Fig 6: Pulmonary Immune Cell Kinetics. Kinetics at 4 h and 24 h pbi of neutrophils (A-B), inflammatory macrophages (C-D), and alveolar macrophages (E-F) from mice infected with PBS (mock) (Panels A, C, E) or 75 $TCID_{50}$ PR8 (Panels B, D, F) followed 7 d later with 10^6 CFU of the indicated bacteria. Each symbol (circles, squares, or diamonds) represents a single mouse, and the bars are the geometric mean ± standard deviation (SD). Mice were either uninfected (open white), influenza-infected only (solid grey), bacteria-infected (open hashed, colored), or influenza-bacteria coinfected (solid hashed, colored). Cartoons indicating infection status of study group (bacteria alone or virus plus bacteria) are in the upper right corner of each graph. Signficance is indicated as *p<0.05, **p<0.01, ***p<0.005, ****p<0.0001. Flow cytometry gating scheme is shown in Fig S5 and additional cellular dynamics are shown in Fig S6.

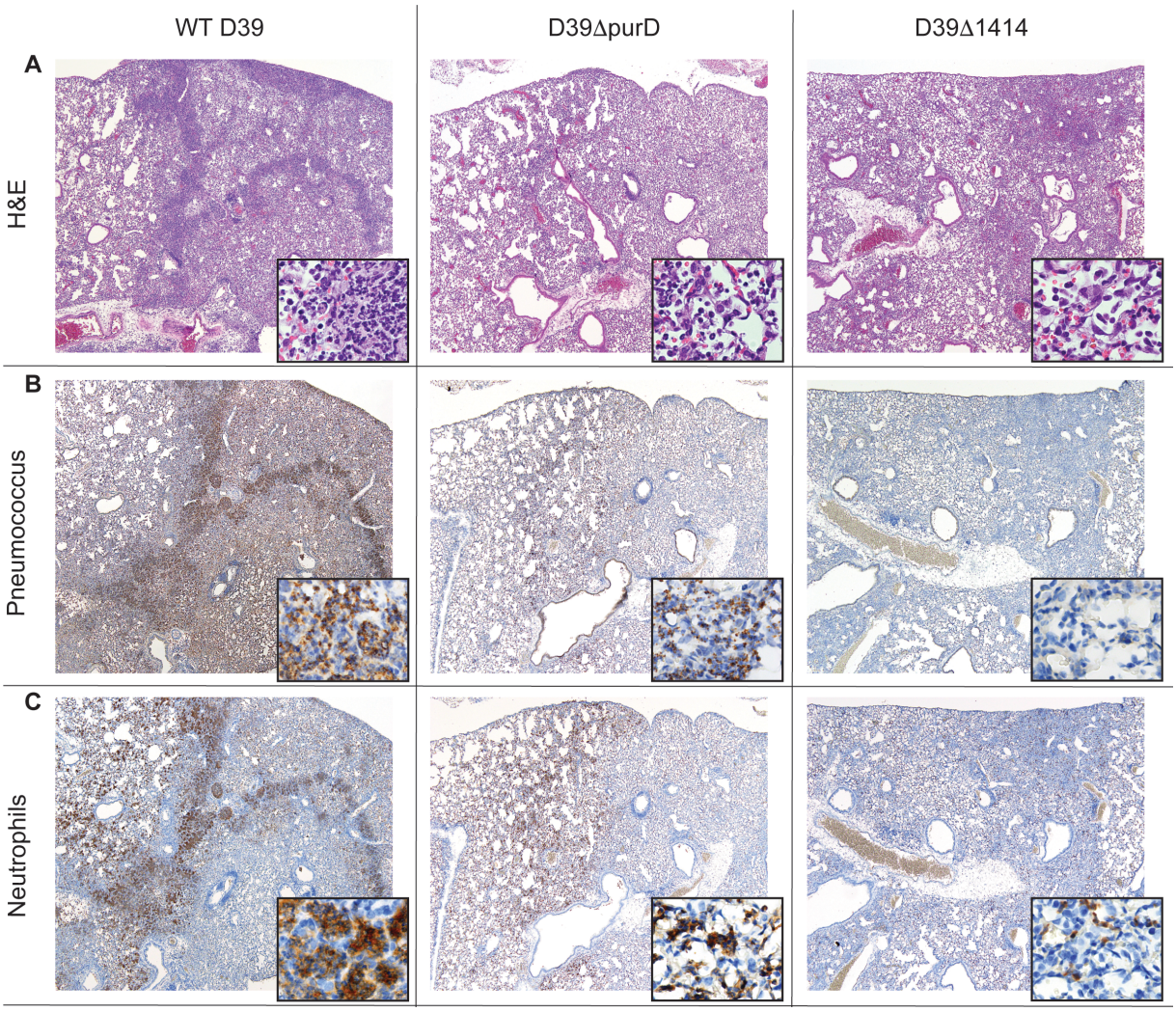

Fig 7: Lung Histology of Coinfection. Histopathology of lung sections collected at 24 h pbi from mice infected with 75 $TCID_{50}$ PR8 followed 7 d later by 10^6 CFU WT D39 or the indicated knockout bacteria. Serial lung sections were stained with hematoxylin and eosin (HE) for histological analysis (Panel A), immunohistochemistry (IHC) for pneumococcus (Panel B), or neutrophils (Panel C). Representative images (original 4x magnification with 60x magnification inset) are shown for WT D39 (left), D39Δ*purD* (middle), *and* D39Δ*1414* (right).

References

1. Brundage JF, Shanks GD. Deaths from Bacterial Pneumonia during 1918–19 Influenza Pandemic. Emerging Infectious Diseases. 2008;14(8):1193-9.
2. Morens DM, Taubenberger JK, Fauci AS. The Persistent Legacy of the 1918 Influenza Virus. New England Journal of Medicine. 2009;361(3):225-9.
3. Klugman KP, Chien Y-W, Madhi SA. Pneumococcal pneumonia and influenza: A deadly combination. Vaccine. 2009;27:C9-C14.
4. Morens David M, Taubenberger Jeffery K, Fauci Anthony S. Predominant Role of Bacterial Pneumonia as a Cause of Death in Pandemic Influenza: Implications for Pandemic Influenza Preparedness. The Journal of Infectious Diseases. 2008;198(7):962-70.
5. Gill JR, Sheng Z-M, Ely SF, Guinee DG, Beasley MB, Suh J, et al. Pulmonary pathologic findings of fatal 2009 pandemic influenza A/H1N1 viral infections. Arch Pathol Lab Med. 2010;134(2):235-43.
6. Weinberger DM, Simonsen L, Jordan R, Steiner C, Miller M, Viboud C. Impact of the 2009 Influenza Pandemic on Pneumococcal Pneumonia Hospitalizations in the United States. The Journal of Infectious Diseases. 2012;205(3):458-65.
7. Louria DB, Blumenfeld HL, Ellis JT, Kilbourne ED, Rogers DE. STUDIES ON INFLUENZA IN THE PANDEMIC OF 1957-1958. II. PULMONARY COMPLICATIONS OF INFLUENZA*†. Journal of Clinical Investigation. 1959;38(1 Pt 1-2):213-65.
8. Gillet Y, Vanhems P, Lina G, Bes M, Vandenesch F, Floret D, et al. Factors Predicting Mortality in Necrotizing Community-Acquired Pneumonia Caused by Staphylococcus aureus Containing Panton-Valentine Leukocidin. Clinical Infectious Diseases. 2007;45(3):315-21.
9. Iverson AR, Boyd KL, McAuley JL, Plano LR, Hart ME, McCullers JA. Influenza virus primes mice for pneumonia from Staphylococcus aureus. The Journal of Infectious Diseases. 2011;203(6):880-8.
10. McCullers Jonathan A, McAuley Julie L, Browall S, Iverson Amy R, Boyd Kelli L, Henriques Normark B. Influenza Enhances Susceptibility to Natural Acquisition of and Disease due to Streptococcus pneumoniae in Ferrets. The Journal of Infectious Diseases. 2010;202(8):1287-95.
11. Smith AM, McCullers JA. Secondary Bacterial Infections in Influenza Virus Infection Pathogenesis. In: Compans RW, Oldstone MBA, editors. Influenza Pathogenesis and Control - Volume I. 385. Cham: Springer International Publishing; 2014. p. 327-56.
12. McCullers JA. The co-pathogenesis of influenza viruses with bacteria in the lung. Nature Reviews Microbiology. 2014;12(4):252-62.
13. Short KR, Habets MN, Hermans PWM, Diavatopoulos DA. Interactions between Streptococcus pneumoniae and influenza virus: a mutually beneficial relationship? Future Microbiology. 2012;7(5):609-24.
14. Rynda-Apple A, Robinson KM, Alcorn JF. Influenza and Bacterial Superinfection: Illuminating the Immunologic Mechanisms of Disease. Infection and Immunity. 2015;83(10):3764-70.
15. Metzger DW, Sun K. Immune Dysfunction and Bacterial Coinfections following Influenza. The Journal of Immunology. 2013;191(5):2047-52.
16. Robinson KM, Kolls JK, Alcorn JF. The immunology of influenza virus-associated bacterial pneumonia. Current Opinion in Immunology. 2015;34:59-67.
17. McAuley JL, Hornung F, Boyd KL, Smith AM, McKeon R, Bennink J, et al. Expression of the 1918 influenza A virus PB1-F2 enhances the pathogenesis of viral and secondary bacterial pneumonia. Cell Host & Microbe. 2007;2(4):240-9.
18. McCullers Jonathan A, Bartmess Kimberly C. Role of Neuraminidase in Lethal Synergism between Influenza Virus and Streptococcus pneumoniae. The Journal of Infectious Diseases. 2003;187(6):1000-9.

19. Smith AM, McCullers JA. Molecular signatures of virulence in the PB1-F2 proteins of H5N1 influenza viruses. Virus Research. 2013;178(1):146-50.
20. Kash JC, Basler CF, García-Sastre A, Carter V, Billharz R, Swayne DE, et al. Global host immune response: pathogenesis and transcriptional profiling of type A influenza viruses expressing the hemagglutinin and neuraminidase genes from the 1918 pandemic virus. Journal of Virology. 2004;78(17):9499-511.
21. Kash JC, Taubenberger JK. The Role of Viral, Host, and Secondary Bacterial Factors in Influenza Pathogenesis. The American Journal of Pathology. 2015;185(6):1528-36.
22. Siegel Steven J, Roche Aoife M, Weiser Jeffrey N. Influenza Promotes Pneumococcal Growth during Coinfection by Providing Host Sialylated Substrates as a Nutrient Source. Cell Host & Microbe. 2014;16(1):55-67.
23. Nishikawa T, Shimizu K, Tanaka T, Kuroda K, Takayama T, Yamamoto T, et al. Bacterial Neuraminidase Rescues Influenza Virus Replication from Inhibition by a Neuraminidase Inhibitor. PLoS ONE. 2012;7(9):e45371.
24. Weeks-Gorospe JN, Hurtig HR, Iverson AR, Schuneman MJ, Webby RJ, McCullers JA, et al. Naturally Occurring Swine Influenza A Virus PB1-F2 Phenotypes That Contribute to Superinfection with Gram-Positive Respiratory Pathogens. Journal of Virology. 2012;86(17):9035-43.
25. Peltola Ville T, Murti KG, McCullers Jonathan A. Influenza Virus Neuraminidase Contributes to Secondary Bacterial Pneumonia. The Journal of Infectious Diseases. 2005;192(2):249-57.
26. McCullers JA, Iverson AR, McKeon R, Murray PJ. The platelet activating factor receptor is not required for exacerbation of bacterial pneumonia following influenza. Scandinavian Journal of Infectious Diseases. 2008;40(1):11-7.
27. Lijek RS, Weiser JN. Co-infection subverts mucosal immunity in the upper respiratory tract. Curr Opin Immunol. 2012;24(4):417-23.
28. Ghoneim HE, Thomas PG, McCullers JA. Depletion of Alveolar Macrophages during Influenza Infection Facilitates Bacterial Superinfections. The Journal of Immunology. 2013;191(3):1250-9.
29. Smith AM, Adler FR, Ribeiro RM, Gutenkunst RN, McAuley JL, McCullers JA, et al. Kinetics of Coinfection with Influenza A Virus and Streptococcus pneumoniae. PLoS Pathogens. 2013;9(3):e1003238.
30. Smith AM, Smith AP. A Critical, Nonlinear Threshold Dictates Bacterial Invasion and Initial Kinetics During Influenza. Scientific Reports. 2016;6(1).
31. Califano D, Furuya Y, Metzger DW. Effects of Influenza on Alveolar Macrophage Viability Are Dependent on Mouse Genetic Strain. J Immunol. 2018;201(1):134-44.
32. Sun K, Metzger DW. Inhibition of pulmonary antibacterial defense by interferon-γ during recovery from influenza infection. Nature Medicine. 2008;14(5):558-64.
33. Janssen WJ, Barthel L, Muldrow A, Oberley-Deegan RE, Kearns MT, Jakubzick C, et al. Fas determines differential fates of resident and recruited macrophages during resolution of acute lung injury. Am J Respir Crit Care Med. 2011;184(5):547-60.
34. Shahangian A, Chow EK, Tian X, Kang JR, Ghaffari A, Liu SY, et al. Type I IFNs mediate development of postinfluenza bacterial pneumonia in mice. Journal of Clinical Investigation. 2009;119(7):1910-20.
35. Tian X, Xu F, Lung WY, Meyerson C, Ghaffari AA, Cheng G, et al. Poly I:C Enhances Susceptibility to Secondary Pulmonary Infections by Gram-Positive Bacteria. PLoS ONE. 2012;7(9):e41879.
36. Karlström Å, Heston SM, Boyd KL, Tuomanen EI, McCullers JA. Toll-Like Receptor 2 Mediates Fatal Immunopathology in Mice During Treatment of Secondary Pneumococcal Pneumonia Following Influenza. The Journal of Infectious Diseases. 2011;204(9):1358-66.

37. McNamee LA, Harmsen AG. Both Influenza-Induced Neutrophil Dysfunction and Neutrophil-Independent Mechanisms Contribute to Increased Susceptibility to a Secondary Streptococcus pneumoniae Infection. Infection and Immunity. 2006;74(12):6707-21.
38. LeVine AM, Koeningsknecht V, Stark JM. Decreased pulmonary clearance of S. pneumoniae following influenza A infection in mice. Journal of Virological Methods. 2001;94(1-2):173-86.
39. Sun K, Metzger DW. Influenza Infection Suppresses NADPH Oxidase-Dependent Phagocytic Bacterial Clearance and Enhances Susceptibility to Secondary Methicillin-Resistant Staphylococcus aureus Infection. The Journal of Immunology. 2014;192(7):3301-7.
40. Abramson JS, Mills EL, Giebink GS, Quie PG. Depression of monocyte and polymorphonuclear leukocyte oxidative metabolism and bactericidal capacity by influenza A virus. Infection and Immunity. 1982;35(1):350-5.
41. Abramson JS, Lewis JC, Lyles DS, Heller KA, Mills EL, Bass DA. Inhibition of neutrophil lysosome-phagosome fusion associated with influenza virus infection in vitro. Role in depressed bactericidal activity. J Clin Invest. 1982;69(6):1393-7.
42. Bansal S, Yajjala VK, Bauer C, Sun K. IL-1 Signaling Prevents Alveolar Macrophage Depletion during Influenza and Streptococcus pneumoniae Coinfection. J Immunol. 2018;200(4):1425-33.
43. Rudd JM, Ashar HK, Chow VT, Teluguakula N. Lethal Synergism between Influenza and Streptococcus pneumoniae. J Infect Pulm Dis. 2016;2(2).
44. McCullers JA. Effect of antiviral treatment on the outcome of secondary bacterial pneumonia after influenza. J Infect Dis. 2004;190(3):519-26.
45. Mitchell AM, Mitchell TJ. Streptococcus pneumoniae: virulence factors and variation. Clinical Microbiology and Infection. 2010;16(5):411-8.
46. Henriques-Normark B, Tuomanen EI. The pneumococcus: epidemiology, microbiology, and pathogenesis. Cold Spring Harb Perspect Med. 2013;3(7).
47. Kadioglu A, Weiser JN, Paton JC, Andrew PW. The role of Streptococcus pneumoniae virulence factors in host respiratory colonization and disease. Nat Rev Microbiol. 2008;6(4):288-301.
48. Wong SM, Bernui M, Shen H, Akerley BJ. Genome-wide fitness profiling reveals adaptations required by Haemophilus in coinfection with influenza A virus in the murine lung. Proceedings of the National Academy of Sciences. 2013;110(38):15413-8.
49. Carter R, Wolf J, van Opijnen T, Muller M, Obert C, Burnham C, et al. Genomic Analyses of Pneumococci from Children with Sickle Cell Disease Expose Host-Specific Bacterial Adaptations and Deficits in Current Interventions. Cell Host & Microbe. 2014;15(5):587-99.
50. van Opijnen T, Bodi KL, Camilli A. Tn-seq: high-throughput parallel sequencing for fitness and genetic interaction studies in microorganisms. Nature Methods. 2009;6(10):767-72.
51. Mohler J, Azoulay-Dupuis E, Amory-Rivier C, Mazoit JX, Bédos JPP, Rieux V, et al. Streptococcus pneumoniae strain-dependent lung inflammatory responses in a murine model of pneumococcal pneumonia. Intensive Care Medicine. 2003;29(5):808-16.
52. Tettelin H. Complete Genome Sequence of a Virulent Isolate of Streptococcus pneumoniae. Science. 2001;293(5529):498-506.
53. Bidossi A, Mulas L, Decorosi F, Colomba L, Ricci S, Pozzi G, et al. A Functional Genomics Approach to Establish the Complement of Carbohydrate Transporters in Streptococcus pneumoniae. PLoS ONE. 2012;7(3):e33320.
54. Titgemeyer F, Hillen W. Global control of sugar metabolism: a gram-positive solution. Antonie Van Leeuwenhoek. 2002;82(1-4):59-71.
55. Deutscher J. The mechanisms of carbon catabolite repression in bacteria. Current Opinion in Microbiology. 2008;11(2):87-93.

159 56. Eisenreich W, Dandekar T, Heesemann J, Goebel W. Carbon metabolism of intracellular
160 bacterial pathogens and possible links to virulence. Nature Reviews Microbiology. 2010;8(6):401-
161 12.
162 57. Paixão L, Caldas J, Kloosterman TG, Kuipers OP, Vinga S, Neves AR. Transcriptional
163 and metabolic effects of glucose on Streptococcus pneumoniae sugar metabolism. Frontiers in
164 Microbiology. 2015;6.
165 58. King SJ. Pneumococcal modification of host sugars: a major contributor to colonization of
166 the human airway? Molecular Oral Microbiology. 2010;25(1):15-24.
167 59. Orihuela CJ, Janssen R, Robb CW, Watson DA, Niesel DW. Peritoneal culture alters
168 Streptococcus pneumoniae protein profiles and virulence properties. Infection and Immunity.
169 2000;68(10):6082-6.
170 60. Orihuela CJ, Radin JN, Sublett JE, Gao G, Kaushal D, Tuomanen EI. Microarray analysis
171 of pneumococcal gene expression during invasive disease. Infect Immun. 2004;72(10):5582-96.
172 61. Ogunniyi AD, Giammarinaro P, Paton JC. The genes encoding virulence-associated
173 proteins and the capsule of Streptococcus pneumoniae are upregulated and differentially
174 expressed in vivo. Microbiology (Reading, Engl). 2002;148(Pt 7):2045-53.
175 62. Ogunniyi AD, Mahdi LK, Trappetti C, Verhoeven N, Mermans D, Van der Hoek MB, et al.
176 Identification of genes that contribute to the pathogenesis of invasive pneumococcal disease by
177 in vivo transcriptomic analysis. Infection and Immunity. 2012;80(9):3268-78.
178 63. LeMessurier KS, Ogunniyi AD, Paton JC. Differential expression of key pneumococcal
179 virulence genes in vivo. Microbiology (Reading, Engl). 2006;152(Pt 2):305-11.
180 64. Mahdi LK, Ogunniyi AD, LeMessurier KS, Paton JC. Pneumococcal virulence gene
181 expression and host cytokine profiles during pathogenesis of invasive disease. Infection and
182 Immunity. 2008;76(2):646-57.
183 65. Honsa ES, Johnson MDL, Rosch JW. The roles of transition metals in the physiology and
184 pathogenesis of Streptococcus pneumoniae. Front Cell Infect Microbiol. 2013;3:92.
185 66. Marion C, Burnaugh AM, Woodiga SA, King SJ. Sialic acid transport contributes to
186 pneumococcal colonization. Infection and Immunity. 2011;79(3):1262-9.
187 67. Robertson L, Caley JP, Moore J. Importance of Staphylococcus aureus in pneumonia in
188 the 1957 epidemic of influenza A. Lancet. 1958;2(7040):233-6.
189 68. Boissy R, Ahmed A, Janto B, Earl J, Hall BG, Hogg JS, et al. Comparative supragenomic
190 analyses among the pathogens Staphylococcus aureus, Streptococcus pneumoniae, and
191 Haemophilus influenzae Using a modification of the finite supragenome model. BMC Genomics.
192 2011;12(1).
193 69. Hiller NL, Janto B, Hogg JS, Boissy R, Yu S, Powell E, et al. Comparative Genomic
194 Analyses of Seventeen Streptococcus pneumoniae Strains: Insights into the Pneumococcal
195 Supragenome. Journal of Bacteriology. 2007;189(22):8186-95.
196 70. Shepardson KM, Larson K, Morton RV, Prigge JR, Schmidt EE, Huber VC, et al.
197 Differential Type I Interferon Signaling Is a Master Regulator of Susceptibility to Postinfluenza
198 Bacterial Superinfection. mBio. 2016;7(3).
199 71. Chandler JD, Hu X, Ko E-J, Park S, Lee Y-T, Orr M, et al. Metabolic pathways of lung
200 inflammation revealed by high-resolution metabolomics (HRM) of H1N1 influenza virus infection
201 in mice. American Journal of Physiology-Regulatory, Integrative and Comparative Physiology.
202 2016;311(5):R906-R16.
203 72. Cui L, Zheng D, Lee YH, Chan TK, Kumar Y, Ho WE, et al. Metabolomics Investigation
204 Reveals Metabolite Mediators Associated with Acute Lung Injury and Repair in a Murine Model
205 of Influenza Pneumonia. Scientific Reports. 2016;6(1).
206 73. Smallwood HS, Duan S, Morfouace M, Rezinciuc S, Shulkin BL, Shelat A, et al. Targeting
207 Metabolic Reprogramming by Influenza Infection for Therapeutic Intervention. Cell Rep.
208 2017;19(8):1640-53.

74. Kroeker AL, Ezzati P, Coombs KM, Halayko AJ. Influenza A Infection of Primary Human Airway Epithelial Cells Up-Regulates Proteins Related to Purine Metabolism and Ubiquitin-Related Signaling. Journal of Proteome Research. 2013;12(7):3139-51.
75. Syk A, Norman M, Fernebro J, Gallotta M, Farmand S, Sandgren A, et al. Emergence of hypervirulent mutants resistant to early clearance during systemic serotype 1 pneumococcal infection in mice and humans. J Infect Dis. 2014;210(1):4-13.
76. Kanehisa M, Furumichi M, Tanabe M, Sato Y, Morishima K. KEGG: new perspectives on genomes, pathways, diseases and drugs. Nucleic Acids Res. 2017;45(D1):D353-D61.
77. Kanehisa M, Goto S. KEGG: kyoto encyclopedia of genes and genomes. Nucleic Acids Res. 2000;28(1):27-30.
78. Kanehisa M, Sato Y, Kawashima M, Furumichi M, Tanabe M. KEGG as a reference resource for gene and protein annotation. Nucleic Acids Res. 2016;44(D1):D457-62.
79. Furuta Y, Takahashi K, Kuno-Maekawa M, Sangawa H, Uehara S, Kozaki K, et al. Mechanism of Action of T-705 against Influenza Virus. Antimicrobial Agents and Chemotherapy. 2005;49(3):981-6.
80. Kiso M, Takahashi K, Sakai-Tagawa Y, Shinya K, Sakabe S, Le QM, et al. T-705 (favipiravir) activity against lethal H5N1 influenza A viruses. Proc Natl Acad Sci U S A. 2010;107(2):882-7.
81. Kloosterman TG, Hendriksen WT, Bijlsma JJE, Bootsma HJ, van Hijum SAFT, Kok J, et al. Regulation of Glutamine and Glutamate Metabolism by GlnR and GlnA in Streptococcus pneumoniae. Journal of Biological Chemistry. 2006;281(35):25097-109.
82. Härtel T, Klein M, Koedel U, Rohde M, Petruschka L, Hammerschmidt S. Impact of Glutamine Transporters on Pneumococcal Fitness under Infection-Related Conditions. Infection and Immunity. 2011;79(1):44-58.
83. Calder PC, Yaqoob P. Glutamine and the immune system. Amino Acids. 1999;17(3):227-41.
84. Castell LM, Bevan SJ, Calder P, Newsholme EA. The role of glutamine in the immune system and in intestinal function in catabolic states. Amino Acids. 1994;7(3):231-43.
85. Newsholme P, Curi R, Gordon S, Newsholme EA. Metabolism of glucose, glutamine, long-chain fatty acids and ketone bodies by murine macrophages. Biochem J. 1986;239(1):121-5.
86. Newsholme P, Gordon S, Newsholme EA. Rates of utilization and fates of glucose, glutamine, pyruvate, fatty acids and ketone bodies by mouse macrophages. Biochem J. 1987;242(3):631-6.
87. Costa Rosa LF, Cury Y, Curi R. Hormonal control of macrophage function and glutamine metabolism. Biochem Cell Biol. 1991;69(4):309-12.
88. Wallace C, Keast D. Glutamine and macrophage function. Metabolism. 1992;41(9):1016-20.
89. Hava DL, LeMieux J, Camilli A. From nose to lung: the regulation behind Streptococcus pneumoniae virulence factors. Mol Microbiol. 2003;50(4):1103-10.
90. Marra A, Asundi J, Bartilson M, Lawson S, Fang F, Christine J, et al. Differential fluorescence induction analysis of Streptococcus pneumoniae identifies genes involved in pathogenesis. Infect Immun. 2002;70(3):1422-33.
91. Obert C, Sublett J, Kaushal D, Hinojosa E, Barton T, Tuomanen EI, et al. Identification of a Candidate Streptococcus pneumoniae core genome and regions of diversity correlated with invasive pneumococcal disease. Infect Immun. 2006;74(8):4766-77.
92. Orihuela CJ, Gao G, Francis KP, Yu J, Tuomanen EI. Tissue-specific contributions of pneumococcal virulence factors to pathogenesis. J Infect Dis. 2004;190(9):1661-9.
93. van Opijnen T, Camilli A. A fine scale phenotype-genotype virulence map of a bacterial pathogen. Genome Res. 2012;22(12):2541-51.

94. Mina MJ, McCullers JA, Klugman KP. Live Attenuated Influenza Vaccine Enhances Colonization of Streptococcus pneumoniae and Staphylococcus aureus in Mice. mBio. 2014;5(1):e01040-13-e-13.
95. Damjanovic D, Lai R, Jeyanathan M, Hogaboam CM, Xing Z. Marked Improvement of Severe Lung Immunopathology by Influenza-Associated Pneumococcal Superinfection Requires the Control of Both Bacterial Replication and Host Immune Responses. The American Journal of Pathology. 2013;183(3):868-80.
96. Schmitz N, Kurrer M, Bachmann MF, Kopf M. Interleukin-1 Is Responsible for Acute Lung Immunopathology but Increases Survival of Respiratory Influenza Virus Infection. Journal of Virology. 2005;79(10):6441-8.
97. Nakamura S, Davis KM, Weiser JN. Synergistic stimulation of type I interferons during influenza virus coinfection promotes Streptococcus pneumoniae colonization in mice. Journal of Clinical Investigation. 2011;121(9):3657-65.
98. Lee B, Robinson KM, McHugh KJ, Scheller EV, Mandalapu S, Chen C, et al. Influenza-induced type I interferon enhances susceptibility to gram-negative and gram-positive bacterial pneumonia in mice. American Journal of Physiology-Lung Cellular and Molecular Physiology. 2015;309(2):L158-L67.
99. Li W, Moltedo B, Moran TM. Type I Interferon Induction during Influenza Virus Infection Increases Susceptibility to Secondary Streptococcus pneumoniae Infection by Negative Regulation of T Cells. Journal of Virology. 2012;86(22):12304-12.
100. Redford PS, Mayer-Barber KD, McNab FW, Stavropoulos E, Wack A, Sher A, et al. Influenza A Virus Impairs Control of Mycobacterium tuberculosis Coinfection Through a Type I Interferon Receptor–Dependent Pathway. The Journal of Infectious Diseases. 2014;209(2):270-4.
101. Högner K, Wolff T, Pleschka S, Plog S, Gruber AD, Kalinke U, et al. Macrophage-expressed IFN-β contributes to apoptotic alveolar epithelial cell injury in severe influenza virus pneumonia. PLoS pathogens. 2013;9(2):e1003188.
102. Blevins LK, Wren JT, Holbrook BC, Hayward SL, Swords WE, Parks GD, et al. Coinfection with Streptococcus pneumoniae Negatively Modulates the Size and Composition of the Ongoing Influenza-Specific CD8 ⁺ T Cell Response. The Journal of Immunology. 2014;193(10):5076-87.
103. Ho SN, Hunt HD, Horton RM, Pullen JK, Pease LR. Site-directed mutagenesis by overlap extension using the polymerase chain reaction. Gene. 1989;77(1):51-9.
104. Horton RM, Cai ZL, Ho SN, Pease LR. Gene splicing by overlap extension: tailor-made genes using the polymerase chain reaction. Biotechniques. 1990;8(5):528-35.
105. Reed LJ, Muench H. A SIMPLE METHOD OF ESTIMATING FIFTY PER CENT ENDPOINTS12. American Journal of Epidemiology. 1938;27(3):493-7.
106. van Opijnen T, Boerlijst MC, Berkhout B. Effects of random mutations in the human immunodeficiency virus type 1 transcriptional promoter on viral fitness in different host cell environments. J Virol. 2006;80(13):6678-85.